This article has been accepted for publication in a future issue of this journal, but has not been fully edited. Content may change prior to final publication. Citation information: DOI 10.1109/TBME.2018.2874716, IEEE Transactions on Biomedical Engineering

A Patient-specific Approach for Short-term Epileptic Seizures Prediction through the Analysis of EEG synchronization

Paolo Detti, Garazi Zabalo Manrique de Lara, Renato Bruni, Marco Pranzo, Francesco Sarnari and Giampaolo Vatti

***Abstract*—Epilepsy is a neurological disorder arising from anomalies of the electrical activity in the brain, affecting about 65 millions individuals worldwide.**

***Objective:* This work proposes a patient-specific approach for short-term prediction (i.e., within few minutes) of epileptic seizures.**

***Methods:* We use noninvasive EEG data, since the aim is exploring the possibility of developing a noninvasive monitoring/control device for the prediction of seizures. Our approach is based on finding synchronization patterns in the EEG that allow to distinguish in real time preictal from interictal states. In practice, we develop easily computable functions over a graph model to capture the variations in the synchronization, and employ a classifier for identifying the preictal state.**

***Results:* We compare two state-of-the-art classification algorithms and a simple and computationally inexpensive threshold-based classifier developed ad hoc. Results on publicly available scalp EEG database and on scalp data of the patients of the Unit of Neurology and Neurophysiology at University of Siena show that this simple and computationally viable processing is able to highlight the changes in synchronization when a seizure is approaching.**

***Conclusion and significance:* The proposed approach, characterized by low computational requirements and by the use of noninvasive techniques, is a step toward the development of portable and wearable devices for real-life use.**

***Index Terms*—EEG analysis; Epilepsy; Synchronization measures; Interaction graph; Data classification.**

I. Introduction

Epilepsy is a neurological disorder affecting about 65 million individuals worldwide [1], with a very high social cost as it results in many injuries (e.g., fractures, burns, accidents and even death). Treatment options for epilepsy are mainly pharmacological and, to a lesser extent, surgical. However, antiepileptic drugs have limitations [2] and fail to control seizures in roughly 20–30% of patients, and surgery is not always possible. In this context, an important issue is the possibility of predicting the occurrences of epileptic seizures (i.e., detecting a pre-ictal or pre-seizure state), in order to take actions to neutralize an incoming seizure or limit the injuries of a seizure occurrence (e.g., by warning alarms, application of short-acting drugs, electrical stimulation).

The possibility of seizure prediction was explored for over 25 years, typically from the analysis of the electroencephalogram (EEG) signals. For recent reviews on this topic, we refer to [3], [4]. Historically, epilepsy has been interpreted as a disorder characterized by abnormally enhanced neuronal excitability and synchronization. Several studies investigated the relationship between seizures and brainwave synchronization patterns, highlighting the possibility of distinguishing: *interictal*, *preictal*, *ictal* and *postictal* states [5], [6], [7]. Furthermore, research in the last few years has replaced the concept of *single epileptic focus* with the concept of *epileptic network* [8], [9], [10], suggesting that a network model of the brain interactions (e.g., measuring the synchronization among different brain areas) appears more appropriate for the description of epilepsy, where the epileptiform activity in any one part is influenced by activity in other parts.

The problem of detecting and/or predicting seizures occurrences can be formulated as a classification problem (see for references, e.g., [11]), and different works from the literature propose solution methods based on classification approaches [5], [12], [13], [14]. Furthermore, the prediction problem is particularly challenging since: (i) the availability of data containing preictal and ictal states is limited; (ii) pre-seizure and seizure morphology may vary both within the same patient (intra-patient specificity) and across different patients (inter-patient specificity); (iii) while in the detection problem the onset of a seizure can be defined with small errors, in the prediction problem, the length of the preictal state is not univocally defined in the literature; (iv) the EEG data usually includes artifacts and noise of different nature.

In this work, we propose a patient-specific classification approach for the short-term prediction of epileptic seizures by detecting synchronization patterns in EEG. The learning steps operate on the specific patient data, so that all the parameters of the procedure can be individually calibrated and the overall approach is able to take into account the inter-patient specificity (as it is also done in [13], [14], [15]). We perform our analysis using noninvasive (scalp) EEG data. Such data generally are noisier than those obtained with other invasive (intracranial) techniques, hence the classification problem becomes more difficult. However, our aim is exploring the possibility of developing of a noninvasive monitoring/control device implementing an expert system for seizure prediction.

P. Detti, G. Zabalo Manrique de Lara, M. Pranzo, F. Sarnari are with the Department of Information Engineering and Mathematics, University of Siena, e-mail {detti,pranzo}@dii.unisi.it, garazizml@gmail.com.

R. Bruni is with the Department of "Ingegneria Informatica, Automatica e Gestionale", University "Sapienza" of Rome, e-mail bruni@dis.uniroma1.it.

G. Vatti is with the Department of Medicine, Surgery and Neuroscience, University of Siena, e-mail giampaolo.vatti@gmail.com.

This article has been accepted for publication in a future issue of this journal, but has not been fully edited. Content may change prior to final publication. Citation information: DOI 10.1109/TBME.2018.2874716, IEEE Transactions on Biomedical Engineering

Hence, the choice of noninvasive techniques would allow an easier real-time use of the proposed method also in portable and wearable devices, possibly able to notify patients and/or caregivers, or to take automatic actions to reduce the injuries, the severity of seizures, or prevent them entirely [13].

The proposed approach is based on finding synchronization patterns in the EEG that allow to distinguish preictal from interictal states. This is obtained by using bivariate measures of synchronization, i.e., measures involving couples of EEG channels. A graph model is built, in which the nodes are associated to the electrodes sites from which the EEG channels are captured, and the edges between two nodes are weighted with the values of one or more synchronization measures (varying over time) of the signals associated to the two nodes. After this, we use easily computable functions over this graph, to capture the variations in the above synchronization. Finally, an automatic classification aims at identifying the preictal state. We compare two state-of-the-art classification algorithms (support vector machines [16] and gradient boosting based on decision trees [17]) and a threshold-based classifier developed ad hoc. We provide extensive results on publicly available EEG data from the "CHB-MIT Scalp EEG Database" [18], [13] and on data of the patients of the Unit of Neurology and Neurophysiology at University of Siena. The experimental campaign, validated through a cross validation scheme, shows a very good prediction capacity and a quite low false alarm rate, on prediction horizons spanning few minutes from the seizure onset.

The main contributions of this work are: (i) The use of recently introduced phase-synchronization measures, namely, Phase Lag Index (*PLI*) and Weighted Phase Lag Index (*WPLI*) [19], [20], to analyze EEG synchronization variations during interictal and preictal states. Although phase synchronization is a topic already investigated for epileptic seizure prediction in the literature (see [4] for a review), *PLI* and *WPLI* have not yet been employed for prediction. (ii) The presentation of a graph model on which we compute simple and computationally inexpensive indices to capture the variations of the synchronization measures over time and space. (iii) To improve the classification results, we propose a modified version of a classical indicator called Moving Average Convergence/Divergence (MACD) [21], commonly used to analyze trends in financial markets, for the feature extraction task. (iv) The introduction of a new, linear and fast threshold-based classification approach developed ad hoc for the problem under study, which exhibits an encouraging performance.

The article is organized as follows. Section II provides the experimental setup and a block diagram of the whole approach. Section III presents the graph model of the brain interactions proposed to study the synchronization patterns. Section IV describes the functions developed to capture the variations in the synchronization patterns. Section V reports our experience in using the classifiers. Section VII provides numerical results on real data from the "CHB-MIT Scalp EEG Database" [18], [13] and from the patients of the Unit of Neurology and Neurophysiology at University of Siena. Conclusions follow in Section VIII.

II. System's architecture

Epileptic seizure prediction approaches usually consist of two main phases. In a first phase (*feature extraction phase*), a number of measures and indices, generically called features, are computed from the physiological signals (e.g., EEG signals) extracted over time. In a second phase (*classification phase*), a classification procedure is applied, in order to identify preictal and interictal states [6], [22] using the time series of the above mentioned features. Since the aim is to anticipate the seizures' occurrences in order to take suitable actions during the preictal period, while at the same time to avoid false positive alarms (i.e., triggering an alarm outside the preictal period), usually the ictal and postictal periods are discarded from the classification.

Features can be extracted from EEG by using univariate measures, i.e., involving a single EEG channel, or by using multivariate measures, involving two or more channels. In the literature, many prediction approaches have been based on univariate measures [23], [24], [22], [25]. However, studies comparing univariate and bivariate measures [26], [27], [6], [5] highlighted the good performance in seizure prediction of the features extracted from bivariate measures.

EEG, especially scalp EEG, is very susceptible to artifacts and noise, producing ictal and preictal-like patterns. The artifact issue is widely discussed in the community, and, since there are no techniques to eliminate them without any elimination of good information, several recent studies (see [26], [28]) consider the raw signal, including the artifacts. This was also done in the present work. However, the following approaches have been used to reduce artifacts' influence: (i) the raw EEG signal has been filtered by a pass-band filter on (narrow) bands experimentally determined; (ii) as already experienced by other authors [29], [22], a differential window is applied to the EEG, with the aim of making preictal signals more distinguishable with respect to interictal ones.

Figure 1 reports the block diagram of the whole approach proposed for the seizure prediction; the feature extraction phase has 6 steps, while the classification phase has 2 steps. All the steps are described below.

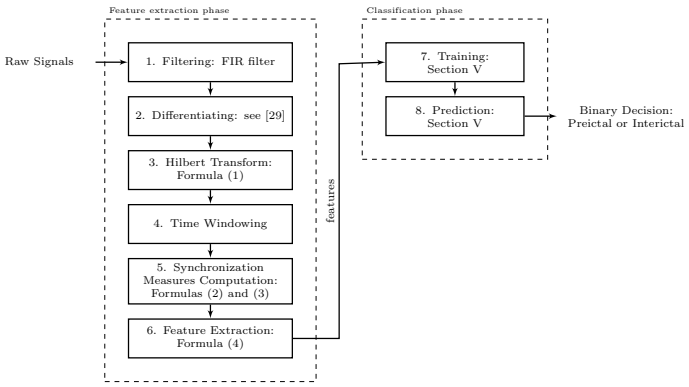

Fig. 1. Block diagram of the proposed approach.

Step 1. The EEG signals are filtered by means of a pass-band FIR filter on pre-specified bands, as detailed in Section VI.

This article has been accepted for publication in a future issue of this journal, but has not been fully edited. Content may change prior to final publication. Citation information: DOI 10.1109/TBME.2018.2874716, IEEE Transactions on Biomedical Engineering

Step 2. The time-derivative of the signals are computed as in [29]. As shown in [29], [22], differentiating makes the basic noise nearly flat and sharpens the regions where the signal exhibits its peaks, which are most likely to be the regions where seizures occur.
Step 3. The analytical signals and their phases are extracted by the Hilbert transform (see Formula (1)) applied to each signal obtained in the previous step.
Step 4. The signals are segmented into consecutive time-windows, possibly overlapping, of N points each.
Step 5. Synchronization measures *PLI* and *WPLI* are computed for each pair of signals and each time-window by Formulas (2) and (3).
Step 6. Features' computation. Features are extracted on each time-window from the synchronization measures. With this aim a graph model is used (Section III-B) and a moving average procedure is applied (see Section IV.)
Step 7. The classification phase is technically composed of a training and a prediction step. It is detailed in Section V. The training step takes data records labeled with a class label (in our case, preictal or interictal) to train the classifier. The training step may optionally be preceded by a feature selection step, that analyzes the set of all available features to select the most promising ones.
Step 8. The prediction step uses the classifier learned in the previous step to assign one of those labels to each new unlabeled record representing the values of the features at each given time. The output of this step is the output of the whole process: a binary decision (preictal or interictal) that can be used to alert the patient of the incoming crisis.

III. EEG SYNCHRONIZATION AND GRAPH REPRESENTATION

In Section III-A, measures of signal synchronization are presented. In Section III-B, the signal synchronization measures are embedded in a graph model of the brain interactions.

A. Measures of the signal synchronization

In this study, phase-synchronization measures of pairs of EEG signals are employed. To compute the phase synchronization, we need to know the instantaneous phase of the two involved signals. This can be extracted by computing the analytical signal. In fact, the analytical signal of a real time series $x(t)$ (such as the signal of an EEG channel) is a complex function $z(t) = x(t) + i\hat{x}(t)$. Function $\hat{x}(t)$ can be computed by the Hilbert Transform as follows:

$$\hat{x}(t) = \frac{1}{\pi} PV \int_{-\infty}^{\infty} \frac{x(\tau)}{t-\tau} d\tau \qquad (1)$$

where PV is the Cauchy principal value. Hence, the transform (1) allows the construction of a complex signal $z(t) = x(t) + i\hat{x}(t) = A(t)e^{i\phi(t)}$, with amplitude $A(t) = \sqrt{[\hat{x}]^2 + [x]^2}$ and phase $\phi(t) = \arctan \frac{\hat{x}(t)}{x(t)}$.

A phase-synchronization measure of EEG signals, called Phase Lag Index (*PLI*), has been introduced in [19], for the assessment of functional connectivity in the brain. *PLI* is based on the idea of discarding the phase differences that center around $0 \pmod{\pi}$. This allows to study short-term changes of increasing and decreasing synchronization [30]. In order to discard the phase differences, an asymmetry index is defined by calculating the likelihood that the phase difference $\Delta\phi$ of two signals will be in the interval $(-\pi, \pi)$. Given the channel pair h, k and a time window Δ_t containing N time instants, *PLI* is formally given by:

$$PLI_{h,k,\Delta_t} = \left| \frac{1}{N} \sum_{p=1}^{N} \text{sign}(\phi_h(p) - \phi_k(p)) \right|, \qquad (2)$$

where $\phi_h(p)$ and $\phi_k(p)$ are the phases of signals at time instant p of channels h and k, respectively, determined by the Hilbert transformation (1). Hence, $0 \leq PLI \leq 1$, and when $PLI = 0$ there is either no coupling or a coupling with a phase difference centered around $0 \pmod{\pi}$, while for $PLI = 1$ a perfect phase locking at a value of $\Delta\phi$ different from $0 \pmod{\pi}$ occurs. The stronger the non zero phase locking is, the larger the *PLI* will be.

In [20], an extension of the *PLI* has been introduced, called Weighted Phase Lag Index (*WPLI*). The *WPLI* index takes values in $[0, 1]$, too, and, in terms of phase difference, can be defined as follows:

$$WPLI_{h,k,\Delta_t} = \frac{\left| \frac{1}{N} \sum_{p=1}^{N} \sin\left(\phi_h(p) - \phi_k(p)\right) \right|}{\frac{1}{N} \sum_{p=1}^{N} \left| \sin\left(\phi_h(p) - \phi_k(p)\right) \right|}. \qquad (3)$$

In *WPLI*, each phase difference is weighted according to the magnitude of the lag. As a consequence, phase differences around zero only marginally contribute to the calculation of the WPLI. This reduces the probability of detecting false positive connectivity in the case of volume conducted noise sources with near zero phase lag, and increases the sensitivity in detecting phase synchronization.
As an example, the upper parts of Figures 2 and 3 show the EEG data of two EEG channels over time (in seconds) of patients $Chb03$ and $Chb05$ of the "CHB-MIT Scalp EEG Database" [18], respectively, as an epileptic seizure is approaching (the seizures start at the vertical dotted lines). For a better view, Figure 4 shows EEG segments of 10 seconds centered at the starting of the seizures (the dotted vertical lines) of the EEGs reported in Figures 2 and 3. For each patient, the channels that better highlight the seizure onset have been selected. Observe that the selected channels for patient $Chb03$ (for patient $Chb05$) are $h = \{F4 - C4\}$ and $k = \{T8 - P8\}$ (are $h = \{T7 - P7\}$ and $k = \{C3 - P3\}$), placed on the right side (left side) of the head. The bottom parts of Figures 2 and 3 show the behavior over the same time span (in seconds) of the EEG data of PLI_{h,k,Δ_t} (solid line) and $WPLI_{h,k,\Delta_t}$ (dotted line) on the selected channels (as computed at Step 5 of Figure 1). *PLI* and *WPLI* are computed using a time window Δ_t of 6 seconds (with an overlap of 1 sec.). Note that, *PLI* and *WPLI* show a rising trend as the seizure is approaching.

Furthermore, Figure 5 shows the behavior over time of *WPLI* for the data of patient $Chb01$ [18], with and without differentiation (i.e., considering or removing Step 2 in the block diagram of Figure 1). We consider the time period of about 1600 seconds before and during the 5^{th} epileptic seizure of the patient (the first and the second vertical dotted lines in

This article has been accepted for publication in a future issue of this journal, but has not been fully edited. Content may change prior to final publication. Citation information: DOI 10.1109/TBME.2018.2874716, IEEE Transactions on Biomedical Engineering

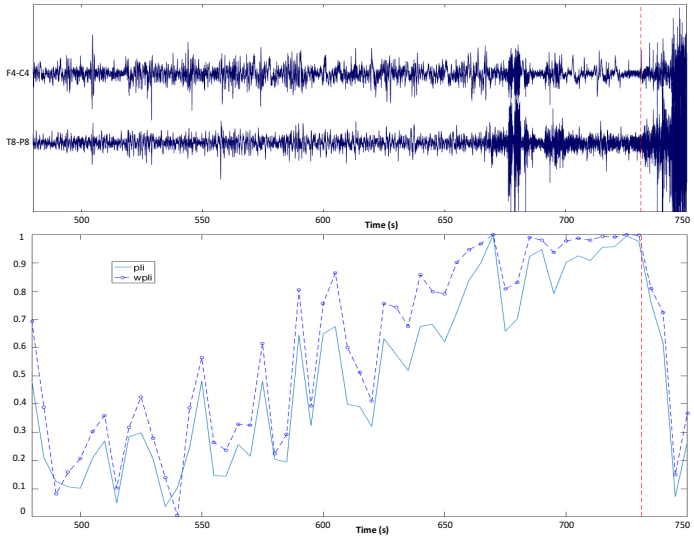

Fig. 2. Raw EEG, $PLI_{h,k}$ and $WPLI_{h,k}$ on channels $h = \{F4 - C4\}$ and $k = \{T8 - P8\}$ on the 2^{nd} seizure of patient $Chb03$.

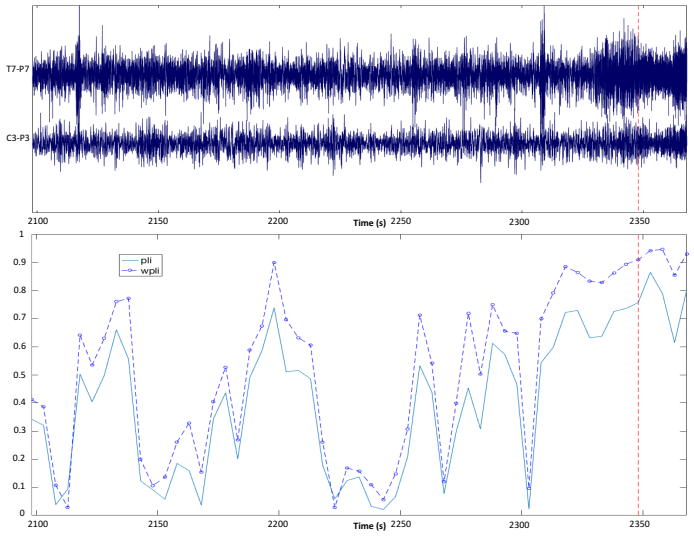

Fig. 3. Raw EEG, $PLI_{h,k}$ and $WPLI_{h,k}$ on channels $h = \{T7 - P7\}$ and $k = \{C3 - P3\}$ on the last seizure of patient $Chb05$.

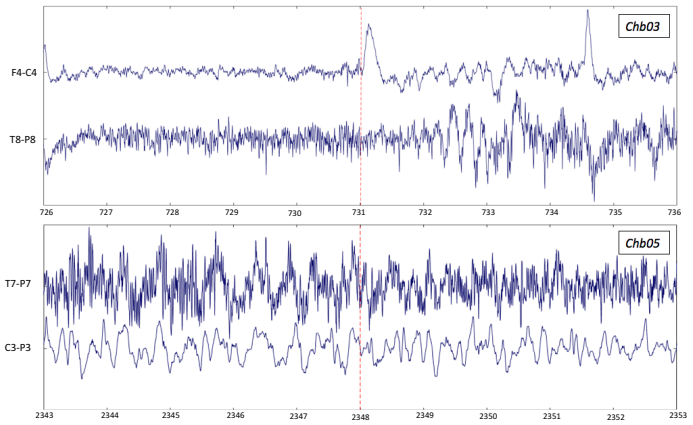

Fig. 4. EEG segments of 10 seconds centered at the starting of the seizures (the dotted vertical lines) of the EEGs reported in Figures 2 and 3.

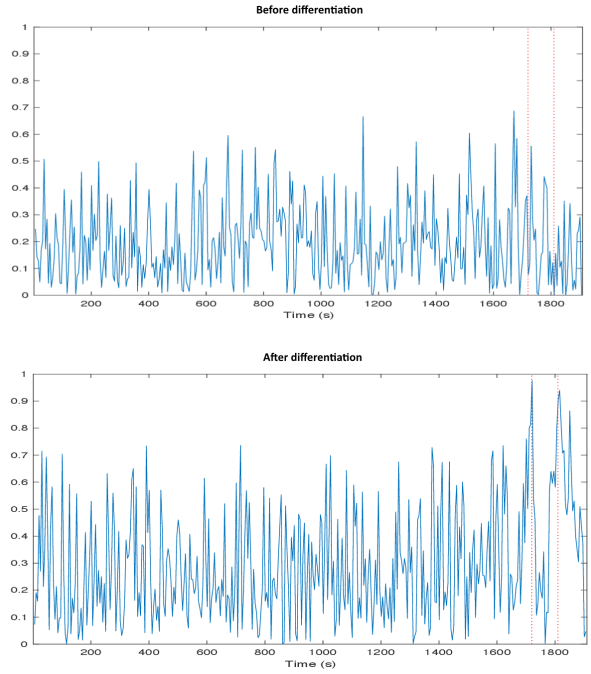

Fig. 5. $WPLI_{h,k}$ with $h = \{P3 - O1\}$ and $k = \{FT9 - FT10\}$ on the 5^{th} epileptic seizure of patient $Chb01$, with and without differentiation.

each figure mark the beginning and the end of the seizure, respectively). $WPLI_{h,k,\Delta_t}$ is computed on the two channels $h = \{P3 - O1\}$ and $k = \{FT9 - FT10\}$ (using a time window Δ_t of 6 seconds with an overlap of 1 second). Note that no apparently significant changes occur in *WPLI* without the application of the differential operator. On the contrary, when using the differentiation, *WPLI* increases as the starting time of the seizure is approaching and has a peak just at the beginning of the seizure (denoted by the first vertical dotted line).

B. Graph model of the brain interactions

The synchronization measures introduced in Section III-A are symmetric values $w_{h,k}$, defined for each pair of channels h and k, i.e., $w_{h,k} = w_{k,h}$. As already observed [31], [20], the EEG signals, i.e., the channels, extracted from the electrodes positioned on the scalp and their connections provide a natural network model of the brain connectivity. Such a network can be modeled by an undirected complete weighted graph $G = (V, A)$, where the nodes represent channels, and an undirected weighted edge $(h, k) \in A$ represents the connection between channels h and k. The weight $w_{h,k}$ associated to the edge $(h, k) \in A$ can be set to the value provided by one of the synchronization measures presented in Section III-A. Note that the synchronization measures and, hence, the edge weights $w_{h,k}$ vary over time. Graph G is a mathematical tool that may help to highlight changes in the neural activity over time, observing how epileptiform events modify the graph structure. Indeed, Graph Theory provides a methodological framework

This article has been accepted for publication in a future issue of this journal, but has not been fully edited. Content may change prior to final publication. Citation information: DOI 10.1109/TBME.2018.2874716, IEEE Transactions on Biomedical Engineering

to develop efficient algorithms on the graph for the detection of particular measures and structures, which can be used for the analysis of synchronization patterns. As observed in [31], two easily computable graph measures of brain connectivity are the *degree* of a node, i.e., the number of edges (with weights larger than a given threshold) incident to a node in G, and the *strength* of a node, i.e., the sum of the weights of the edges incident to a node in G.

As an example, Figure 6 illustrates the evolution of the graph G at several time instants in the approach of an epileptic seizure. More precisely, the data are related to the third seizure of the patient $Chb03$ of the "CHB-MIT Scalp EEG Database" [18], starting at the second 432. Each graph is related to a time window Δ_t of 6 seconds, and edges' weights $w_{h,k}$ measure *PLI* between channels h and k computed over the time window Δ_t by Formula (2). For a better view, only edges with $w_{h,k}$ larger than 0.7 are reported and the nodes, i.e., the channels, have been positioned around a circle. Observe that the number of edges with high weights increases in the two time windows (the graphs in Figures 6.(d) and 6.(e)) immediately before the seizure (the graph in Figure 6.(f)), implying an increase in synchronization. Figure 7 reports the behavior over time of the

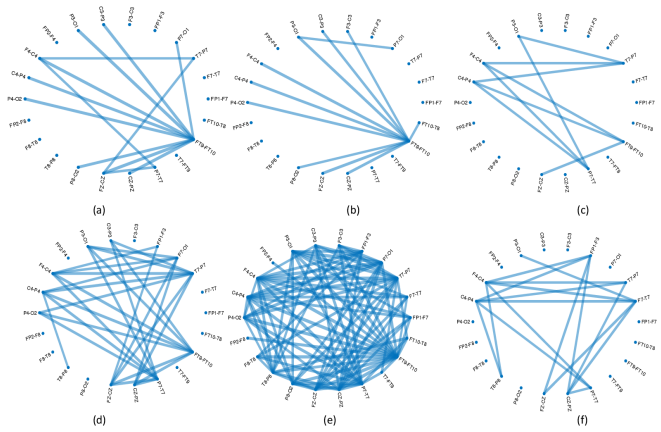

Fig. 6. (a) G related to $\Delta_t = [390, 396]$; (b) G related to $\Delta_t = [394, 400]$; (c) G related to $\Delta_t = [404, 410]$; (d) G related to $\Delta_t = [414, 420]$; (e) G related to $\Delta_t = [424, 430]$; (f) G related to $\Delta_t = [429, 435]$.

node's strength related to node/channel $P7 - O1$, computed by *PLI*, on a time period of about 600 seconds containing the third seizure of patient $Chb03$, starting at the second 432). The two vertical dotted lines delimit the ictal period. Note that the strength of the node increases as the ictal period is approaching and then decreases. The period immediately preceding the ictal period is called preictal period. Its length is not defined in general. Thus, in our experiments, we consider the length of the preictal period as a parameter and we call it *prediction interval*.

IV. Feature Extraction

The prediction of a seizure from the analysis of the synchronization measures introduced in Section III could already be viewed as a classification problem. However, to successfully use a classification algorithm, we should integrate and/or

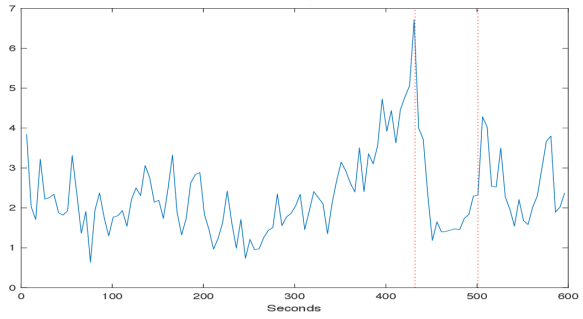

Fig. 7. Strength for Channel $P7 - O1$.

elaborate the features directly extracted from the EEG data, i.e., the synchronization measures, with additional information derived from them. This additional information should basically inform the classifier, in each time instant, about the relation occurring at that time between the current value of the features and their past values considered at an aggregate level, otherwise this information would not be available to the classifier. More specifically, to allow a reliable detection of a preictal state, it could be useful to define functions that should be able to highlight the particular (rising) trends in the synchronization measures which could be precursors of a seizure occurrence (see Figures 2 and 3). In what follows, we propose indicators based on moving average techniques, which may be of help in the detection of the above described trends in the synchronization measures of the EEG data.

Let us denote each of the measure computed in the previous section (i.e., PLI_{h,k,Δ_t} or $WPLI_{h,k,\Delta_t}$) by $f_{h,k}(\Delta_t)$. We resort to the following functions:
a) A function $T_{h,k}(\Delta_t)$ describing the *trend* of the generic measure $f_{h,k}(\Delta_t)$ at time period Δ_t.
b) A function $L_{h,k}(\Delta_t)$ representing a *current lower limit* of the above $T_{h,k}(\Delta_t)$ in a time window representing the recent past with respect to time period Δ_t.
c) A function $M_{h,k}(\Delta_t)$ measuring the *elevation* of the current trend above the current lower limit at time period Δ_t, to detect whether a rising trend occurs for a sufficient interval of time.

a) Choice of the trend function $T_{h,k}(\Delta_t)$: A moving average, i.e., the average over a certain time interval of the values of $f_{h,k}(\Delta_t)$, is generally chosen to describe trends. A weighted moving average (WMA) has multiplying factors to give different weights to the different instants of time. Usually, recent instants receive more importance than older ones. In particular, an exponential moving average (EMA) applies weighting factors which decrease exponentially in the past, using a parameter w representing the extension of the past. In our case, we chose for the trend function $T_{h,k}(\Delta_t)$ an EMA, computed as follows:

$$T_{h,k}(\Delta_t) = \begin{cases} f_{h,k}(1) & \text{for } t = 1 \\ \left(\frac{2}{w+1}\right) f_{h,k}(\Delta_t) + \left(1 - \frac{2}{w+1}\right) T_{h,k}(\Delta_t - 1) & \text{for } t > 1 \end{cases}$$

We experimentally find that $w = 7$ provides a good trend description in our application.

This article has been accepted for publication in a future issue of this journal, but has not been fully edited. Content may change prior to final publication. Citation information: DOI 10.1109/TBME.2018.2874716, IEEE Transactions on Biomedical Engineering

b) Choice of the current lower limit $L_{h,k}(\Delta_t)$: To evaluate the current lower limit, we chose the minimum of $T_{h,k}(\Delta_t)$ over the previous p time intervals.

$$L_{h,k}(\Delta_t) = \min_{\tau \in \{\Delta_t - p, \ldots, \Delta_t\}} \{T_{h,k}(\tau)\}$$

We experimentally find that p = 27 provides a satisfactory lower limit in our application.

c) Choice of the elevation function $M_{h,k}(\Delta_t)$: In this case, we follow the ideas underlying the trading indicator called Moving Average Convergence/Divergence (MACD) [21]. The simplest version of MACD is the difference between two moving averages, one over a shorter time interval and one over a longer time interval. Indeed, when the trend is increasing, the moving average over the shorter interval becomes the greater one. Conversely, the same moving average becomes the smaller one when the trend is decreasing. Further insight can be obtained by using a third moving average of the MACD itself over an even shorter interval, called "signal line".

However, to detect the particular kind of rising trend that in our application represents a preictal situation, we experienced better accuracy by substituting the longer-period average with the current lower limit $L_{h,k}(\Delta_t)$. This allows to highlight not only the "relative" information of the changes in the trend of a measure $f_{h,k}(\Delta_t)$, but also the more "absolute" information of the amplitude of the elevation of that measure over the current low value. We call this difference Moving Average and Amplitude Convergence/Divergence (MAACD), computed as:

$$M_{h,k}(\Delta_t) = T_{h,k}(\Delta_t) - L_{h,k}(\Delta_t). \quad (4)$$

In conclusion, we compute the described MAACD for each measure $f_{h,k}(\Delta_t)$, and we use MAACD as features to perform the classification. As an example, Figure 8 shows the function MAACD computed over the *WPLI* reported in Figure 5.b As can be noted, MAACD rises as the seizure is approaching.

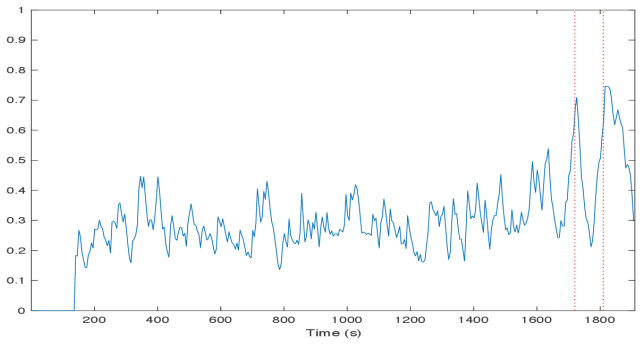

Fig. 8. MAACD computed on $WPLI_{h,k}$ with $h = \{P3 - O1\}$ and $k = \{FT9 - FT10\}$ on the 5^{th} epileptic seizure of patient $Chb01$.

V. Classification

This section describes the classification approaches used to predict the preictal states. We tested two different classification algorithms from the literature, namely a Support Vector Machine (SVM) algorithm [16] and a Gradient Boosting Decision Tree algorithm called *LightGBM* [17]. Furthermore, we present and test a computationally inexpensive threshold-based classification algorithm specifically designed for this problem, called *ThAlgo*. Indeed, in the case of on-line seizure prediction operated by means of wearable, small devices, with necessarily limited power, the low computational requirements would be highly desirable.

For all the classification algorithms, the MAACD features $M_{h,k}(\Delta_t)$ (4) introduced in Section IV have been employed. As stated at the end of Section III-B, given a dataset possibly containing seizures, the *prediction interval* is a time window immediately preceding each seizure (not univocally defined in the literature), that constitutes the time period in which we would like to obtain the alarm for the incoming crisis. Records inside (outside) the prediction interval constitute the positive (negative) class. We allow the use of different values of prediction interval, receiving them as input of our procedures. When the classifier is applied to an unlabeled dataset to operate the prediction, the positive classification of at least one record inside a given prediction interval means that the corresponding seizure has been successfully predicted. The *prediction time* of a seizure is computed as the distance between the first positive record inside the prediction interval of a seizure and its onset. On the contrary, the positive classification of a record outside the defined prediction intervals is counted as a false positive.

Observe that the cardinalities of the two classes in the datasets are very different, with the positive records being generally less than 1%. Thus, this is a very imbalanced case of classification problem, and this makes the classification task more difficult. To face this issue, classification algorithms may allow the attribution of weights to the classes.

A. Support Vector Machines

SVMs are supervised learning models that build a deterministic linear classifier. They are based on finding a separating hyperplane that maximizes the margin between the extreme training data of opposite classes. New examples are then mapped into that same space and predicted to belong to a class, on the basis of which side of the hyperplane they fall on. In addition to performing linear classification, SVMs can efficiently perform a non-linear classification using what is called the kernel trick, by implicitly mapping their inputs to a higher dimensional space, see also [16]. This classifier requires to set some algorithmic parameters, in particular when using as kernel a Gaussian radial basis function. The main parameters in this case are the penalty parameter c of the error term and the kernel coefficient γ. Moreover, the weights assigned to the classes become for this imbalanced problem another main parameter for SVM classifiers. Very roughly, weights should be inversely proportional to the cardinalities of the two classes. In our experiments, the exact values of parameters and weights have been determined by means of a grid search technique, choosing the combination of values (for parameters and weights) that constitute a good compromise between crisis prediction and number of false alarms, determined patient by patient. We use the SVM implementation provided in [32].

This article has been accepted for publication in a future issue of this journal, but has not been fully edited. Content may change prior to final publication. Citation information: DOI 10.1109/TBME.2018.2874716, IEEE Transactions on Biomedical Engineering

B. Gradient Boosting Decision Tree algorithms

Gradient Boosting frameworks are based on decision tree algorithms, and are widely used for classification tasks due to their efficiency and accuracy. Gradient boosting trains an ensemble of simple estimators (i.e., decision trees). The training is done in sequence and in each iteration the training process aims at minimising the residual errors. State-of-the-art Gradient Boosting implementations [33], [17] make use of a number of improvements to attain more accurate results and faster predictions, and are used in classification and machine learning applications. *LightGBM* [17] is an efficient implementation of a Gradient Boosting Decision Tree algorithm.

C. Threshold-based classification approach

The threshold-based approach *ThAlgo* uses a feature selection phase before the classification phase. Feature selection may in general exploit a variety of search techniques to identify the subsets of features that are the most *relevant* for the classification task, possibly providing a measure which scores the different subsets.

In *ThAlgo*, the selection phase has two steps. In the first step, a set of thresholds $\theta_{h,k}$ is obtained, one for each of the MAACD features $M_{h,k}(\Delta_t)$ (4). In practice, threshold $\theta_{h,k}$ is computed as the average of $M_{h,k}(\Delta_t)$ over the prediction intervals (or a suitable subset of it) of the training data. In the second step, two different rankings of these MAACD features are computed. In the first ranking, the features are sorted in descending order of the number of times each feature $M_{h,k}(\Delta_t)$ has a value above its threshold $\theta_{h,k}$ inside the prediction intervals. This ranking basically evaluates, for each feature, its ability in the identification of positive records, i.e., those corresponding to preictal states. In the second ranking, the features are sorted in descending order of the number of times each feature $M_{h,k}(\Delta_t)$ has a value below its threshold $\theta_{h,k}$ outside the prediction intervals. Hence, it basically evaluates the ability in not producing false positive predictions of the negative records, i.e., those corresponding to interictal states. The indices of the features topping the first ranking constitute the set S_1; the indices of the features topping the second ranking constitute S_2. The cardinalities of S_1 and S_2 can be selected, and they represent parameters of the algorithm.

In the subsequent classification phase, all the selected features $M_{h,k}(\Delta_t)$ and their corresponding thresholds $\theta_{h,k}$ are linearly combined to obtain a single feature $M(\Delta_t)$ and a corresponding single threshold Θ, as follows:

$$M(\Delta_t) = \sum_{(h,k)\in S_1} \alpha_{h,k} M_{h,k}(\Delta_t) + \sum_{(h,k)\in S_2} \alpha_{h,k} M_{h,k}(\Delta_t) \quad (5)$$

$$\Theta = \sum_{(h,k)\in S_1} \alpha_{h,k} \theta_{h,k} + \sum_{(h,k)\in S_2} \alpha_{h,k} \theta_{h,k} \quad (6)$$

where the weights $\alpha_{h,k}$, with $(h,k) \in S_1 \cup S_2$, are parameters of the algorithm. The classification is performed by evaluating, on the test data set, whenever the combined feature $M(\Delta_t)$ (6) is above (below) its threshold Θ inside (outside) the prediction intervals. In our experiments, two features are selected in the selection phase, namely the first feature of each ranking. Hence, $|S_1| = |S_2| = 1$.

VI. Data description and experimental setup

This section describes the EEG data used in our experiments and the main preprocessing steps. Two sets of data have been considered. The first set contains data of the patients of the "CHB-MIT Scalp EEG Database" [18], [13], which consists of bipolar scalp EEG recordings from 23 pediatric subjects (18 females and 5 males) with intractable seizures from the Children's Hospital Boston. The age of the patients ranges from 1.5 to 22 years. No other clinical information is available for the data of this set. All signals are sampled at 256 Hz using the International 10–20 system of EEG electrode positions. The dataset of each patient is composed of a number of instances, generally lasting about 1 hour each. Some are seizure instances, i.e., they contain at least a seizure occurrence, the other are nonseizure instances. To prepare the data for our prediction task, each seizure instance (1 hour long in most of the cases) is fractioned into (sub-)instances, each containing a single seizure, in which we discarded: all the ictal periods (i.e., the periods between the onset and the ending time of each seizure); the time period preceding the onset of a seizure of more than 1 hour, if any; a (postictal) period of 1000 seconds after the end of each seizure. Then, all the seizure instances obtained so far with a preictal period smaller than 300 seconds have been removed from the dataset. (As a consequence, a seizure is not considered if, in the original seizure instance, a preceding seizure exists, such that the period of time between the end of the preceding seizure and the beginning of the current seizure is smaller than 1300 seconds.) Furthermore, for each patient, we only considered recordings (i.e., instances) with the same EEG montage and the same number of EEG channels. All the nonseizure instances (with the same EEG montage and the same number of channels) have been considered for each patient. No subsampling of the data has been performed. The second set contains data acquired from 7 patients admitted to the Unit of Neurology and Neurophysiology, Department of Neurological and Neurosensorial Sciences, University of Siena. The patients were monitored with a Video-EEG with a sampling rate of 512 Hz, with electrodes arranged on the basis of the international 10-20 system. The diagnosis of epilepsy and the classification of seizures according to the criteria of the International League Against Epilepsy [34] (reported in Table II) were performed by an expert clinician after a careful revision of the clinical and electrophysiological data of each patient. The data in this set have been subsampled at 256 Hz and segmented into seizure and nonseizure instances according to the criteria described above. Tables I and II reports detailed overviews of the two sets of data. Table II also reports the clinical information for the second set of data (Columns 2–6). Columns 2 and 3 of Table I and Columns 7 and 8 of Table II show, for each patient, the number of EEG channels (n) and seizures (Seiz.).

In the classification phase, for each patient, we use a cross validation approach, which is a statistical technique to assess

This article has been accepted for publication in a future issue of this journal, but has not been fully edited. Content may change prior to final publication. Citation information: DOI 10.1109/TBME.2018.2874716, IEEE Transactions on Biomedical Engineering

the quality of a prediction model. More precisely, let m be the total number of instances of a patient dataset, and let m_s and m_{ns} be the number of seizure instances (resulting by the data selection described above) and the number of nonseizure instances, respectively ($m = m_s + m_{ns}$). The total number of instances used for training is $m_{train} = \lfloor 0.6m \rfloor$ (i.e., no more than 60% of the overall patient's dataset). The training set is obtained by randomly selecting $\lceil 0.5m_s \rceil$ seizure instances and $m_{train} - \lceil 0.5m_s \rceil$ nonseizure instances. As a consequence, the testing is performed on $m - m_{train}$ instances, of which $m_s - \lceil 0.5m_s \rceil$ are seizure instances. Columns 4 and 5 of Table I and Columns 9 and 10 of Table II report the number of seizures used in the training phase and in the test phase respectively.

For each patient, q rounds of cross validation have been performed, with the additional condition that each seizure instance is selected for testing in at least one of the q rounds. Parameter q has been set equal to 5 for patients such that $m_s \geq 4$ and equal to 3 when $m_s = 3$. Observe that three out of the 23 patients of the CHB-MIT database cannot be included (i.e., Chb02, Chb11, Chb19) since they have only 2 seizures and do not allow a reasonable definition of training and testing sets for cross validation. Finally, Columns 6 and 7 of Table I and Columns 11 and 12 of Table II report the average number of EEG hours over the q rounds of cross validation used in the training phase and in the test phase respectively.

According to a preliminary analysis in which different settings have been tested, in the feature extraction phase (see Figure 1) we operated the following steps on each data set: (i) EEG signals are filtered using a band-pass FIR filter with band [8–13] Hz; (ii) The synchronization measures presented in Section III-A have been computed for each channel pair on a time window $\Delta_t = 6$ secs with an overlap of 1 sec. No additional artifact suppression method is used.

Two sets of features have been evaluated. The first set contains the MAACD functions (4), denoted as $M_{h,k}(\Delta_t)$ and $M'_{h,k}(\Delta_t)$, computed over the two synchronization measures $PLI_{h,k}(\Delta_t)$ and $WPLI_{h,k}(\Delta_t)$, respectively. Then, this set contains two features for each channel pair (h, k), with $h, k = 1, \ldots, n$, $h \neq k$, i.e., for each arc of the graph G introduced in section III-B. The second set contains the strengths of each channel k (i.e., node k of graph G) related to the same MAACD functions (4), i.e., $2n$ features in total. More formally, the two strengths at node k are defined as $\sum_{h=1,h\neq k}^{n} M_{h,k}(\Delta_t)$ and $\sum_{h=1,h\neq k}^{n} M'_{h,k}(\Delta_t)$.

In all the classification algorithms, in the training and test phase we consider prediction intervals of length T. In the training phase, we set to True the records of a time window ranging from T seconds before each seizure onset till the actual onset of the seizure. All the other records are set to False (interictal). In our experiments, three different lengths of T have been considered: $T \in \{150, 200, 300\}$ seconds.

VII. Experimental results

This section reports on our experiments on the data of the patients described in Section VI. Table III shows the results obtained by the three classification algorithms *ThAlgo*, *LightGBM* and *SVM* on the data of Table I. Table VI reports the results attained by *ThAlgo* on the second data set. All the results are average over the q runs of the cross validation scheme described in Section VI, with $q \in \{3; 5\}$. Since our approach is patient specific, results are computed choosing for each patient the combination of the classifier parameters giving the best performance. The performance is measured in terms of correctly predicted seizures and rate of false alarms. A seizure is correctly predicted if at least a record inside the correspondent prediction interval is classified as true. In the test phase, we considered the prediction time t_p of a seizure as the difference between the onset of the seizure marked in the database and the time of the first record inside the correspondent prediction interval classified as true. A positive value of t_p indicates how early a seizure is predicted. In order to evaluate the systems' behavior in terms of false alarms, we compute the specificity (true-negative rate) and the false positive rate computed as $TN/(FP + TN) \times 100$ and $FP/(FP+TN) \times 100$, respectively, where TN and FP are the number of true negative and false positives records, respectively. More precisely, a record classified as true outside all the prediction intervals produces a false positive, while a record classified as negative outside all the prediction intervals is a true negative.

In Table III, each row reports the average results of the cross validation related to each of the considered patients of the CHB-MIT database for the three classification algorithms. The last row of the table shows the overall average results. The first column of the table reports the patient's id. Then, for each algorithm, "F." is the feature set on which the best (average) results are obtained ("A" denotes all arcs of the graph G, "N" denotes nodes' strengths), $pred\%$ is the percentage of seizures of the test set correctly predicted, $spec\%$ is the specificity and $fpr\%$ is the false positive rate. Furthermore, $\bar{t}_p$, t_p^m and t_p^M respectively are the average, the minimum and the maximum prediction time in seconds, computed over all the seizures of the the q runs of the cross validation scheme. We observe that algorithm *ThAlgo* correctly predicts all the seizures ($pred\% = 100$), while *LightGBM* has a prediction rate of 98% and *SVM* of 86.7%. *LightGBM* attains the best specificity (and hence the best false positive rate) on average, more than 96%, while *ThAlgo* and *SVM* get a specificity of 95.97% and 95%, respectively. Note that, in our experimental settings, a specificity of 99.87% corresponds to less than 1 false positive per hour (0.94 to be precise), because our features are computed over a time window (i.e., an epoch) Δ_t of 6 seconds with one second of overlap, that is 720 samples per hour. Such an encouraging false positive frequency is obtained in several cases by our classifiers. In fact, as can be noted in Table III, all together, *LightGBM* and *ThAlgo* produce less than 1 false positive per hour on 8 out of the tested 20 patients. *LightGBM* has the biggest average, minimum and maximum prediction time, equal to 124.24, 25.5 and 208.75 seconds on average, respectively. *ThAlgo* and *SVM* provide about 79 and 109 average prediction time (in seconds), respectively. Generally, those prediction times (ranging from about 1.3 to 2 minutes, on average) appear to be sufficient, for a real-time use of the proposed system, for taking actions to reduce the injuries. In fact, although a short-term prediction horizon may

This article has been accepted for publication in a future issue of this journal, but has not been fully edited. Content may change prior to final publication. Citation information: DOI 10.1109/TBME.2018.2874716, IEEE Transactions on Biomedical Engineering

Pat. id	n	Seiz.	Train Seiz.	Test Seiz.	Train hours	Test hours
Chb01	22	7	4	3	22.63	15.08
Chb03	22	7	4	3	19.74	14.03
Chb04	22	4	2	2	83.86	57.6
Chb05	22	5	3	2	21.62	14.78
Chb06	22	10	5	5	29.73	18.82
Chb07	22	3	2	1	34.17	26.76
Chb08	22	5	3	2	11.16	7.46
Chb09 (2nd channel set)	22	4	2	2	39.59	22.51
Chb10	22	7	4	3	25.31	16.58
Chb12 (1st and 4th channel set)	22	9	5	4	8.82	5.8
Chb13 (4th and 6th channel set)	22	7	4	3	3.61	3.47
Chb14	22	8	4	4	14.11	9.44
Chb15 (2nd channel set)	31	13	7	6	17.37	12.04
Chb16 (1st channel set)	22	5	3	2	8.14	5.81
Chb17 (1st channel set)	22	3	2	1	11.56	7.78
Chb18 (2nd channel set)	22	5	3	2	18.7	13.2
Chb20	22	5	3	2	13.49	10.6
Chb21	22	4	2	2	18.16	13.2
Chb22	22	3	2	1	17.44	12.72
Chb23	22	6	3	3	13.88	7.58

TABLE I
DATA OF THE PATIENTS OF THE "CHB-MIT SCALP EEG DATABASE".

Pat. Id	Age (years)	Gender	Type of seizure	Localization	Lateralization	n	Seiz.	Train Seiz.	Test Seiz.	Train hours	Test hours
1	55	Male	IAS	T	R	29	5	3	2	0.86	0.54
2	10	Female	IAS	T	L	31	3	2	1	2.93	1.96
3	24	Male	IAS	T	L	31	5	3	2	5.45	4.05
4	16	Male	FBTC	All	All	30	8	4	4	6.69	4.44
5	9	Male	IAS	T	L	30	4	2	2	3.15	2.17
6	34	Female	IAS	T	L	31	3	2	1	4.08	3.09
7	19	Male	WIAS	T	L	31	4	2	2	8.84	6.92

IAS: focal onset impaired awareness; WIAS: focal onset without impaired awareness; FBTC: focal to bilateral tonic–clonic; T: temporal; R: right, L: left.

TABLE II
DATA OF THE PATIENTS OF THE UNIT OF NEUROLOGY AND NEUROPHYSIOLOGY AT UNIVERSITY OF SIENA.

	ThAlgo						*LightGBM*						*SVM*					
Pat.	F.	pred%	spec%	$\bar{t}_p$	t_p^m	t_p^M	F.	pred%	spec%	$\bar{t}_p$	t_p^m	t_p^M	F.	pred%	spec%	$\bar{t}_p$	t_p^m	t_p^M
Chb01	A	100	98.73	29.4	0	122	A	100	99.98	32	0	105	N	100	100	28.65	5	70
Chb03	A	100	99.53	47.13	14	158	N	100	99.87	53.33	15	145	N	100	97.07	115	10	195
Chb04	A	100	97.41	42.1	0	115	A	59.8	98.35	62.3	0	195	N	40	98.82	160	100	205
Chb05	A	100	100	66.7	21	143	N	100	100	58.5	5	150	N	100	99.98	146	45	240
Chb06	N	100	91.74	198.48	9	293	N	100	92.79	223.2	35	295	N	80	95.72	143.25	5	195
Chb07	A	100	99.94	29.33	0	49	N	100	99.65	100	20	195	N	66	99.75	92.5	30	155
Chb08	A	100	99.34	51.2	0	210	N	100	98.77	57.5	10	125	N	90	98.85	44.4	30	60
Chb09	A	100	99.29	12.3	0	35	A	100	99.98	160	40	295	N	100	99.92	136.5	85	295
Chb10	N	100	100	39	19	70	A	100	99.98	84.67	0	145	N	100	99.74	108	35	195
Chb12	A	100	71.41	243.95	22	292	A	100	80.62	230.25	0	295	N	90	75.72	264.4	165	295
Chb13	A	100	83.49	221.67	47	291	N	100	86.5	218	110	295	N	93.33	69.22	241.4	175	295
Chb14	A	100	95.1	42.35	0	113	N	100	90.63	169	25	295	N	90	89.23	69.7	0	140
Chb15	A	100	93.77	178.3	8	295	A	100	95.82	153.17	0	295	N	90	98.47	85.55	15	145
Chb16	A	100	97.9	102.7	12	218	A	100	95.81	241.5	20	295	N	70	97.72	63.55	15	90
Chb17	A	100	98.66	76.67	19	175	N	100	98.05	213.33	110	280	N	66	98.99	22.5	15	30
Chb18	A	100	99.91	38.1	14	49	N	100	99.45	80.5	15	170	N	90	99.57	51.65	0	115
Chb20	A	100	95.84	28.6	0	82	A	100	95.87	70	5	135	N	100	91.46	101	0	195
Chb21	A	100	99.35	52.3	4	128	A	100	99.41	52.5	0	145	N	100	96.37	72	10	150
Chb22	A	100	100	17	1	32	A	100	100	138.33	100	175	N	100	99.98	110	55	160
Chb23	A	100	98.04	60.07	9	142	N	100	92.98	86.67	0	145	N	86.66	93.42	131.15	10	195
Av.		100	95.97	78.87	9.95	150.6		97.99	96.23	124.24	25.5	208.75		87.6	95	109.36	40.25	171

TABLE III
PERFORMANCES OF THE CLASSIFICATION ALGORITHMS ON THE DATA OF THE "CHB-MIT SCALP EEG DATABASE".

not be enough to guarantee long-acting antiepilectic drugs to take effect, it enables patients to find a safe position, while at the same time not ruining the quality of life. In practice, even in case of a false positive, the patient after few minutes of wait can resume her previous activities. Note that, in some cases, the algorithms obtain $t_p^m = 0$, i.e., at least one seizure in the test set has been detected at the onset. Algorithms *ThAlgo* and *LightGBM* have been tested both on the first and the second set of features. As it results from columns 2 and 8 of Table III, *ThAlgo* attains the best performances mainly on the first set of features (i.e., on the arcs of graph G), while in *LightGBM* there is not a prominence of a features' set with respect to the other. *SVM* has been only tested on the nodes' strengths, because the higher computational demand of the parameters choice in the training step does not allow to run this classifier on the larger first set of features with times compatible for a real time use. Table IV reports a more detailed analysis of the results of Table III. The table shows the Positive Predictive Value (PPV) of the three classification approaches, computed as $TP/(TP + FP) \times 100$, where TP is the number of true positive records (i,e., records inside the prediction intervals classified as true). For taking into account the imbalanceness of the data between positive and negative records, we also report in Table IV a new measure that we call Balanced Positive Predictive Value (BPPV), computed as $TP/P/(TP/P + FP/N) \times 100$, where P is the total number of positive records and N is the total number of negative records. In the last column, Imb. is the percentage of positive records with respect to the total number of records, computed considering the maximum prediction interval (of 300 seconds). We observe that, data are highly unbalanced (Imb. is 5.45% on average) due to a prevalance of negative records over positive records. Hence, PPV ranges from 28 to 33% on average. However, BPPV attains higher values (about 77% on average). In the literature, the CHB-MIT database has been used both for seizure detection, see [35], [13], [14], [36], and for seizure prediction, see [39], [38], [37], [15]. However, few works adopt a cross validation scheme to evaluate the performances

This article has been accepted for publication in a future issue of this journal, but has not been fully edited. Content may change prior to final publication. Citation information: DOI 10.1109/TBME.2018.2874716, IEEE Transactions on Biomedical Engineering

	ThAlgo		*LightGBM*		*SVM*		
Pat.	PPV	BPPV	PPV	BPPV	PPV	BPPV	Imb.
Chb01	11.36	76.51	92.08	99.66	100	100	3.91
Chb03	33.14	94.65	57.43	98.48	11.23	81.86	4.19
Chb04	1.32	82.23	15.05	97.86	1.64	74.13	0.58
Chb05	100	100	100	100	91.60	99.74	2.83
Chb06	4.12	46.35	4.74	50.01	7.65	71.77	4.95
Chb07	36.54	98.93	5.21	89.81	12.58	95.84	0.93
Chb08	26.07	86.05	11.20	68.82	20.94	87.63	5.65
Chb09	5.63	88.92	87.05	99.78	63.58	99.15	1.48
Chb10	100	100	94.62	99.90	53.03	97.94	3.54
Chb12	5.83	31.07	12.94	52.00	6.05	31.94	13.52
Chb13	12.11	41.21	8.48	32.04	5.59	23.16	19.12
Chb14	5.21	60.48	3.85	34.96	4.48	56.64	7.15
Chb15	18.58	70.85	27.63	80.26	38.62	93.35	9.32
Chb16	9.75	59.31	6.77	49.51	17.76	85.81	7.30
Chb17	12.60	81.61	2.69	45.95	5.08	77.03	3.21
Chb18	55.67	98.33	10.14	84.09	26.98	95.87	3.19
Chb20	1.87	49.03	2.68	58.13	3.69	59.07	3.94
Chb21	19.69	90.55	16.72	94.08	6.15	79.49	2.54
Chb22	90	99.85	100	100	84.62	99.76	1.97
Chb23	21.44	84.77	5.89	56.07	10.58	64.03	9.73
Av.	28.55	77.04	33.26	74.57	28.59	78.71	5.45

TABLE IV
PPV AND BPPV RESULTS RELATED TO THE RESULTS OF TABLE III.

Study	# of patients	Cross Val.	Prediction Horizon	pred%	spec%	Pred. Time
van Esbroeck *et al.*[14] (detection)	23	leave-one-out	-	100	76.86	-
Samiee *et al.* [35] (detection)	24	-	-	71.6	99.2	-
Xiang *et al.* [36] (detection)	18	10-fold	-	98.27	98.36	-
Zandi *et al.* [15] (prediction)	3	-	40 min	83.81	99.93	16.13 min
Myers *et al.* [37] (prediction)	10	-	60 min	77	90.00	-
Chu *et al.* [38] (prediction)	13	-	85.5 min	89.19	99.88	49.51 min
Alotaiby *et al.* [39] (prediction)	24	leave-one-out	60, 90, 120 min	85.6	49.67	53.25 min
Proposed approach: *ThAlgo* (prediction)	20	5-fold	150, 200, 300 sec	100	95.97	1.31 min
Proposed approach: *LightGBM* (prediction)	20	5-fold	150, 200, 300 sec	97.99	96.23	2.07 min

TABLE V
COMPARISON WITH PUBLISHED WORKS USING THE "CHB-MIT SCALP EEG DATABASE" FOR SEIZURE DETECTION AND PREDICTION.

Pat.	pred%	spec%	PPV	BPPV	$\bar{t}_p$	t_p^m	t_p^M	Imb.
1	100	100	100	100	142.80	29	213	52.58
2	100	98.20	8.75	99.96	29.67	15	37	11.73
3	100	95.46	22.79	99.99	152.50	0	294	9.89
4	100	96.28	20.67	99.98	94.90	0	290	13.49
5	90	96.63	41.28	99.99	221.67	0	292	13.64
6	100	100	100	100	67	1	157	7.67
7	80	98.06	23.56	100	131.50	0	289	4.77
Av.	95.71	97.81	45.29	99.99	120	6.43	224.57	16.25

TABLE VI
PERFORMANCES OF *Thalgo* ON THE DATA OF THE UNIT OF NEUROLOGY AND NEUROPHYSIOLOGY AT UNIVERSITY OF SIENA.

of the classification obtained [39], [14], [36], and in any case the experimental settings differ considerably in the different works. For example, the set of patients, the length of epochs (in which the data are segmented for features' extraction and classification), the methods for choosing the training and the test data are different. Thus, a fair comparison between the different approaches cannot be directly performed. The performances are often measured in terms of number of false positives per hour, however this indicator strongly depends on the length of the epochs (i.e., the time window Δ_t) used for extracting the features, and hence from the number of samples contained in one hour. For this reason, we use the specificity as a more reliable performance measure. Moreover, the shorter prediction horizon used in our short-term approach inevitably produces smaller prediction times and higher false positive rates than the other longer-term prediction approaches. Therefore, a direct comparison of this aspect is not easy.

Table VII shows a comparison of the best results of our approach (obtained with *ThAlgo* and *LightGBM*) with other works from the literature addressing seizure detection or prediction. For each work, we report the number of tested patients of the CHB-MIT database, the type of cross validation, if any, the prediction horizon, the sensitivity ($pred\%$, i.e., the percentage of predicted seizures), the specificity ($spec\%$) and the average prediction time. When not provided, we derived the specificity from the average number of false positives per hour and the epoch's length.

Observe that our *ThAlgo* and *LightGBM* algorithms achieve the best sensitivity for seizure prediction (i.e., the percentage of correctly classified seizures), while the two proposed algorithms have a specificity of about 96%, smaller than the ones obtained in [38], [15] (that use a smaller set of patients without a cross validation scheme). As already stated, our prediction times are smaller than the other prediction approaches, ranging from about 1.3 to 2 minutes, on average. On the other hand, we point out that a seizure predictor with too long prediction times introduces an uncertainty on the right time for taking the suitable actions (e.g., resting in a safe position), and could be of limited practical interest for an everyday use.

Table VI reports the results for *ThAlgo* on the data of Table II, using the feature set "A" only. Also in this case, data are unbalanced (Imb. 16% on average). Note that, *ThAlgo* performs better with respect to the results of the first dataset with the only exception of the prediction rate (about 95.7%).

VIII. CONCLUSIONS

This work presents a patient-specific approach for the prediction of epileptic seizures, based on finding synchronization patterns in the EEG signals. At this aim, a graph model of the brain interactions and an easily computable function have been proposed. Three binary classification approaches have been tested: a simple threshold-based classifier tailored for our application, and two classifiers from the literature (i.e.,

a Gradient Boosting Decision Tree and a Support Vector Machine algorithm). Computational tests on real data from the "CHB-MIT Scalp EEG Database" [18] and from the Unit of Neurology and Neurophysiology at University of Siena show that the computationally viable threshold-based approach proposed in this work is able to effectively detect the changes in the synchronization corresponding to the preictal state a few minutes before the seizure onset. With the aim of developing portable and wearable devices for real-life use, future research directions include: (i) evaluation of different graph measures; (ii) development of more sophisticated methods to compute the thresholds in the linear classifier; (iii) testing our approach on larger EEG scalp datasets; (iv) integration of the features considered here with other features derived from different physiological signals (e.g., EKG signals) to limit the artifact influence and improve effectiveness and reliability of the classification phase; (v) real-world data acquisition and real-time application of the proposed classifiers.

ACKNOWLEDGEMENTS

The authors thank the two anonymous Reviewers for their valuable suggestions and comments. The research has been partially supported by the grant "PANACEE" (Prevision and analysis of brain activity in transitions: epilepsy and sleep) of the Regione Toscana - PAR FAS 2007-2013 1.1.a.1.1.2 - B22I14000770002.

REFERENCES

[1] *Epilepsy Foundations*, Last accessed on February 27th, 2018, https://www.epilepsy.com/.

[2] C. Deckers *et al.*, "Current limitations of antiepileptic drug therapy: a conference review," *Epilepsy research*, vol. 53, no. 1-2, pp. 1–17, 2003.

[3] E. B. Assi *et al.*, "Towards accurate prediction of epileptic seizures: A review," *Biomedical Signal Processing and Control*, vol. 34, pp. 144–157, 2017.

[4] K. Gadhoumi *et al.*, "Seizure prediction for therapeutic devices: A review," *Journal of neuroscience methods*, vol. 260, pp. 270–282, 2016.

[5] P. Mirowski *et al.*, "Classification of patterns of eeg synchronization for seizure prediction," *Clinical neurophysiology*, vol. 120, no. 11, pp. 1927–1940, 2009.

[6] F. Mormann *et al.*, "On the predictability of epileptic seizures," *Clinical neurophysiology*, vol. 116, no. 3, pp. 569–587, 2005.

[7] ——, "Mean phase coherence as a measure for phase synchronization and its application to the eeg of epilepsy patients," *Physica D: Nonlinear Phenomena*, vol. 144, no. 3-4, pp. 358–369, 2000.

[8] M. A. Kramer and S. S. Cash, "Epilepsy as a disorder of cortical network organization," *The Neuroscientist*, vol. 18, no. 4, pp. 360–372, 2012.

[9] L. Lemieux *et al.*, "Concepts of connectivity and human epileptic activity," *Frontiers in systems neuroscience*, vol. 5, p. 12, 2011.

[10] F. Wendling *et al.*, "From intracerebral eeg signals to brain connectivity: identification of epileptogenic networks in partial epilepsy," *Frontiers in systems neuroscience*, vol. 4, p. 154, 2010.

[11] R. Bruni and G. Bianchi, "Effective classification using a small training set based on discretization and statistical analysis," *IEEE Transactions on Knowledge and Data Engineering*, vol. 27, no. 9, pp. 2349–2361, 2015.

[12] L. Chisci *et al.*, "Real-time epileptic seizure prediction using ar models and support vector machines," *IEEE Transactions on Biomedical Engineering*, vol. 57, no. 5, pp. 1124–1132, 2010.

[13] A. H. Shoeb, "Application of machine learning to epileptic seizure onset detection and treatment," Ph.D. dissertation, Massachusetts Institute of Technology, 2009.

[14] A. Van Esbroeck *et al.*, "Multi-task seizure detection: addressing intra-patient variation in seizure morphologies," *Machine Learning*, vol. 102, no. 3, pp. 309–321, 2016.

[15] A. S. Zandi *et al.*, "Predicting epileptic seizures in scalp eeg based on a variational bayesian gaussian mixture model of zero-crossing intervals," *IEEE Transactions on Biomedical Engineering*, vol. 60, no. 5, pp. 1401–1413, 2013.

[16] C.-C. Chang and C.-J. Lin, "Training v-support vector classifiers: theory and algorithms," *Neural computation*, vol. 13, no. 9, pp. 2119–2147, 2001.

[17] G. Ke *et al.*, "Lightgbm: A highly efficient gradient boosting decision tree," in *Advances in Neural Information Processing Systems*, 2017, pp. 3149–3157.

[18] *CHB-MIT Scalp EEG Database*, Last accessed on February 27th, 2018, http://physionet.org/pn6/chbmit/.

[19] C. J. Stam *et al.*, "Phase lag index: assessment of functional connectivity from multi channel eeg and meg with diminished bias from common sources," *Human brain mapping*, vol. 28, no. 11, pp. 1178–1193, 2007.

[20] M. Vinck *et al.*, "An improved index of phase-synchronization for electrophysiological data in the presence of volume-conduction, noise and sample-size bias," *Neuroimage*, vol. 55, no. 4, pp. 1548–1565, 2011.

[21] G. Appel, *Technical analysis: power tools for active investors*. FT Press, 2005.

[22] M. Z. Parvez and M. Paul, "Epileptic seizure prediction by exploiting spatiotemporal relationship of eeg signals using phase correlation," *IEEE Transactions on Neural Systems and Rehabilitation Engineering*, vol. 24, no. 1, pp. 158–168, 2016.

[23] W. A. Chaovalitwongse *et al.*, "Novel optimization models for abnormal brain activity classification," *Operations Research*, vol. 56, no. 6, pp. 1450–1460, 2008.

[24] R. Esteller *et al.*, "Continuous energy variation during the seizure cycle: towards an on-line accumulated energy," *Clinical Neurophysiology*, vol. 116, no. 3, pp. 517–526, 2005.

[25] J. Rasekhi *et al.*, "Preprocessing effects of 22 linear univariate features on the performance of seizure prediction methods," *Journal of neuroscience methods*, vol. 217, no. 1-2, pp. 9–16, 2013.

[26] M. Bandarabadi *et al.*, "Epileptic seizure prediction using relative spectral power features," *Clinical Neurophysiology*, vol. 126, no. 2, pp. 237–248, 2015.

[27] L. Kuhlmann *et al.*, "Patient-specific bivariate-synchrony-based seizure prediction for short prediction horizons," *Epilepsy research*, vol. 91, no. 2-3, pp. 214–231, 2010.

[28] K. Gadhoumi *et al.*, "Discriminating preictal and interictal states in patients with temporal lobe epilepsy using wavelet analysis of intracerebral eeg," *Clinical neurophysiology*, vol. 123, no. 10, pp. 1906–1916, 2012.

[29] K. K. Majumdar and P. Vardhan, "Automatic seizure detection in ecog by differential operator and windowed variance," *IEEE Transactions on Neural Systems and Rehabilitation Engineering*, vol. 19, no. 4, pp. 356–365, 2011.

[30] M. Winterhalder *et al.*, "The seizure prediction characteristic: a general framework to assess and compare seizure prediction methods," *Epilepsy & Behavior*, vol. 4, no. 3, pp. 318–325, 2003.

[31] M. Rubinov and O. Sporns, "Complex network measures of brain connectivity: uses and interpretations," *Neuroimage*, vol. 52, no. 3, pp. 1059–1069, 2010.

[32] F. Pedregosa *et al.*, "Scikit-learn: Machine learning in python," *Journal of machine learning research*, vol. 12, no. Oct, pp. 2825–2830, 2011.

[33] T. Chen and C. Guestrin, "Xgboost: A scalable tree boosting system," in *Proceedings of the 22nd acm sigkdd international conference on knowledge discovery and data mining*. ACM, 2016, pp. 785–794.

[34] F. *et al.*, "Operational classification of seizure types by the international league against epilepsy: Position paper of the ilae commission for classification and terminology." *Epilepsia*, vol. 58, pp. 522–530, 2017.

[35] K. Samiee *et al.*, "Epileptic seizure detection in long-term eeg records using sparse rational decomposition and local gabor binary patterns feature extraction," *Knowledge-Based Systems*, vol. 118, pp. 228–240, 2017.

[36] J. Xiang *et al.*, "The detection of epileptic seizure signals based on fuzzy entropy," *Journal of neuroscience methods*, vol. 243, pp. 18–25, 2015.

[37] M. H. Myers *et al.*, "Seizure prediction and detection via phase and amplitude lock values," *Frontiers in human neuroscience*, vol. 10, p. 80, 2016.

[38] H. Chu *et al.*, "Predicting epileptic seizures from scalp eeg based on attractor state analysis," *Computer methods and programs in biomedicine*, vol. 143, pp. 75–87, 2017.

[39] T. N. Alotaiby *et al.*, "Epileptic seizure prediction using csp and lda for scalp eeg signals," *Computational intelligence and neuroscience*, vol. 2017, 2017.